Reduced-order modeling and control of bioinspired inline swimming

Rose Gebhardt
Department of Aerospace Engineering
University of Maryland
College Park, Maryland, USA
rgebhard@umd.edu

Derek A. Paley
Department of Aerospace Engineering
and Institute for Systems Research
University of Maryland
College Park, Maryland, USA
dpaley@umd.edu

***Abstract*—This paper presents a nonlinear feedback control design to stabilize the configuration of two swimmers moving inline in a uniform flow. We use a control-theoretic analysis of an experimentally validated model of inline swimming to characterize the behavior and stable points of the open-loop system. We find a linear control law that manipulates the flapping phase offset to stabilize the swimmers to a desired inline separation distance. We identify an idealized Hamiltonian version of the system and use it to find a nonlinear control law to improve the convergence rate of the linear control law. A combination of the two control laws stabilizes the system to a specified configuration faster than the natural dynamics.**

***Index Terms*—bioinspiration, hydrodynamics, Lyapunov-based control, Hamiltonian dynamics**

I. Introduction

Bioinspired robotic fish benefit from greater propulsion efficiency than traditional propeller-based autonomous underwater vehicles (AUVs) [1]–[3]. Robotic fish exhibit enhanced stealthiness attributed to their minimal acoustic signature and inconspicuous wake structure, features particularly valuable in defense applications [4]. Schooling principles have also been applied to underwater gliders for ocean sampling [5], although not for hydrodynamic benefits as considered here.

To better understand the flow interactions between schooling fish, kinematic models of linear arrays of flapping foils have been developed and experimentally validated. This work shows that inline swimming promotes group cohesion [6]–[8]. Additionally, stable configurations of two self-propelled flapping filaments form as a result of vortex shedding of the leader [9]. Experimental testing of bioinspired robotic fish in constant speed flow shows that hydrodynamic benefits of inline swimming are achieved when the distance between the fish varies linearly with the flapping phase offset [10]. Feedback control has also been applied to stabilize frequency uncoordinated swimmers to a cohesive formation [11].

To study inline swimming interactions between fish, we produce a dynamic model of the inline separation distance and determine the equilibrium points and stability properties of the system. We implement a linear control law and then utilize an idealized Hamiltonian system that exists near the equilibrium points to derive a nonlinear feedback control law that stabilizes the two fish to a set distance from one another.

The specific contributions of this paper are (1) a dynamical systems analysis of an experimentally validated model of inline swimming motion; (2) the identification of an idealized Hamiltonian system and a candidate Lyapunov function for nonlinear control design; and (3) a feedback control law that stabilizes two swimmers at a prescribed separation distance with faster convergence rate than the natural dynamics; This work has applications in bioinspired underwater vehicle design and maritime applications with multiple vehicles.

The outline of this paper is as follows. Section II introduces an experimentally validated model of inline swimming behavior and describes the equation of motion. Section III provides control-theoretic analysis of the natural dynamics to characterize the location and stability of equilibrium points. Section IV derives a linear feedback control that is locally capable of stabilizing trajectories to a desired inline separation distance. Section V derives a nonlinear control law to stabilize an idealized system and shows results of the closed-loop system. Section VI summarizes the key findings and discusses ongoing and future work.

II. Theoretical Background

This section introduces the inline swimming system that was described and validated by Newbolt et al. [6]. It provides modeling assumptions and a second-order resultant equation of motion for the inline swimming separation distance.

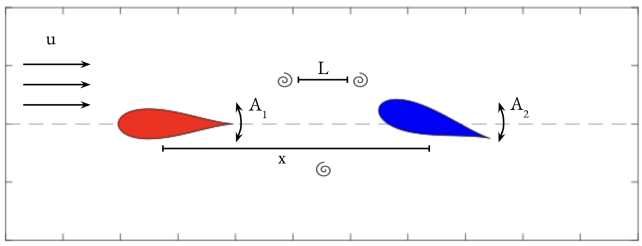

Fig. 1: System schematic: the upstream swimmer's (red) wake interacts with the downstream swimmer (blue).

A. System Definition

Consider two inline swimmers separated by a horizontal distance $x(t)$, as shown in Figure 1, where $x(t)$ increases in the downstream direction.

Assume the swimmers flap at the same frequency, f, but with tail amplitudes A_1 for the upstream swimmer and A_2 for the downstream swimmer; the flapping phase offset is ϕ.

The vertical displacements of the upstream and downstream swimmer's tail, $y_1(t)$ and $y_2(t)$, respectively, are [6]

$$\begin{aligned} y_1(t) &= \frac{1}{2}A_1 \sin(2\pi f t) \\ y_2(t) &= \frac{1}{2}A_2 \sin(2\pi f t - \phi). \end{aligned}$$

We approximate the shape of both fish as an uncambered hydrofoil with chord length c, span s, coefficient of drag C_D, coefficient of thrust C_T, and mass m in a fluid of density ρ. The thrust T_1 and drag D_1 on the upstream swimmer are [6]

$$\begin{aligned} T_1 &= \frac{1}{2}\rho c s C_T \dot{y}_1^2 = \frac{1}{2}\rho c s C_T A_1^2 f^2 \pi^2 \cos^2(2\pi f t) \\ D_1 &= \frac{1}{2}\rho c s C_D \dot{x}_1^2. \end{aligned}$$

Applying Newton's second law to the upstream swimmer gives the equation of motion [6]

$$\ddot{x}_1 = \frac{D_1 - T_1}{m} = \frac{\rho c s}{2m}\left[-C_T A_1^2 f^2 \pi^2 \cos^2(2\pi f t) + C_D \dot{x}_1^2\right].$$

Let $\langle\cdot\rangle$ denote the operation $\langle\cdot\rangle = \int_0^{f^{-1}} (\cdot)\mathrm{d}t$, which returns the time-average value over one flapping period. Assume that the time-averaged upstream velocity is constant, i.e., $\langle \dot{x}_1 \rangle = -U$. The choice of sign convention is consistent with the fact that the foils propel themselves upstream in the negative x direction. Applying the relation $C_D = \pi^2 \mathrm{St}^2 C_T/2$ [6], where the Strouhal number $\mathrm{St} = fA/U$ is the dimensionless parameter describing oscillatory flows, simplifies the equations of motion to $\langle \ddot{x}_1 \rangle = 0$.

Next, to calculate the thrust T_2 and drag D_2 on the downstream swimmer, assume an idealized vortex shedding pattern. The distance between like-signed vortices shed by the upstream swimmer is $L = U/f$ and the vortex strength does not dissipate over time. The time averaged thrust $\langle T_2 \rangle$ and drag $\langle D_2 \rangle$ on the downstream swimmer are [6]

$$\begin{aligned} \langle T_2 \rangle &= \frac{\rho c s C_T f^2 \pi^2}{4}\left[A_2^2 + A_1^2 - 2A_1 A_2 \cos(2\pi f \Delta t - \phi)\right] \\ \langle D_2 \rangle &= \frac{1}{2}\rho c s C_D \operatorname{sgn}(-\langle \dot{x}_2 \rangle)\langle \dot{x}_2 \rangle^2, \end{aligned}$$

where $\Delta t = x/U$ is the time elapsed since the upstream swimmer passed the downstream swimmer's current position. Using these relations along with the equations for St and C_D, Newton's second law applied to the time-averaged downstream swimmer yields the equation of motion $\langle \ddot{x}_2 \rangle = \frac{1}{m}(\langle D_2 \rangle - \langle T_2 \rangle)$ or [6]

$$\begin{aligned} \langle \ddot{x}_2 \rangle = \frac{\rho c s C_T f^2 \pi^2}{4m}\Bigg[&\left(\frac{A_1}{U}\right)^2 \operatorname{sgn}(-\langle \dot{x}_2 \rangle)\langle \dot{x}_2 \rangle^2 \\ &- A_2^2 - A_1^2 + 2A_1 A_2 \cos\left(\frac{2\pi x}{L} - \phi\right)\Bigg]. \end{aligned} \quad (1)$$

Finally, combining the dynamics of the upstream and downstream swimmers yields the behavior of the time-averaged inline separation distance. Let x refer to the time-averaged separation distance, i.e., $x = \langle x_2 \rangle - \langle x_1 \rangle$. Then $\dot{x} = \langle \dot{x}_2 \rangle - \langle \dot{x}_1 \rangle = \langle \dot{x}_2 \rangle + U$ and $\ddot{x} = \langle \ddot{x}_2 \rangle$.

These relationships can be used to convert (1) into the following second-order differential equation in x:

$$\begin{aligned} \ddot{x} = \frac{\rho c s C_T f^2 \pi^2}{4m}\Bigg[&\left(\frac{A_1}{U}\right)^2 \operatorname{sgn}(U - \dot{x})(\dot{x} - U)^2 \\ &- A_2^2 - A_1^2 + 2A_1 A_2 \cos\left(\frac{2\pi x}{L} - \phi\right)\Bigg]. \end{aligned}$$

Applying the definition of the Strouhal number and choosing the substitutions $a = \rho c s C_T \pi^2 \mathrm{St}^2 U^2/4m$ and $A = 2A_1/A_2$. yields the equation of motion

$$\begin{aligned} \ddot{x} = \frac{4a}{A^2}\Bigg[&\frac{A^2}{4}\operatorname{sgn}\left(1 - \frac{\dot{x}}{U}\right)\left(1 - \frac{\dot{x}}{U}\right)^2 - 1 - \frac{A^2}{4} \\ &+ A\cos\left(\frac{2\pi x}{L} - \phi\right)\Bigg]. \end{aligned} \quad (2)$$

The next section provides a dynamical system interpretation and analysis of (2), which represents a substantial reduction in the dimensionality of the original fluid dynamics.

III. Open-Loop Dynamics

This section applies a control-theoretic analysis to the model (2) to characterize local behavior near equilibrium conditions. The insights gained from this analysis are used in designing a control law in Sections IV and V.

A. State-Space System and Equilibrium Points

The components of (2) are caused by the drag and thrust on the downstream swimmer, i.e., $\ddot{x} = d(\dot{x}) - \tau(x, \phi)$, where $d(\dot{x})$ and $\tau(x, \phi)$ are

$$d(\dot{x}) = a \operatorname{sgn}\left(1 - \frac{\dot{x}}{U}\right)\left(1 - \frac{\dot{x}}{U}\right)^2 \quad (3)$$

$$\tau(x, \phi) = \frac{4a}{A^2}\left[1 + \frac{A^2}{4} - A\cos\left(\frac{2\pi x}{L} - \phi\right)\right]. \quad (4)$$

Recall that ϕ is the phase shift of the follower's tail flapping. To obtain a state-space model of the system, let the state vector ζ be $\zeta = \left(x, \dot{x}\right)^T$. Then the state-space form of (2) is

$$\begin{aligned} \dot{\zeta}_1 &= \zeta_2 \\ \dot{\zeta}_2 &= d(\zeta_2) - \tau(\zeta_1, \phi). \end{aligned} \quad (5)$$

To find the equilibrium points ζ^* such that $\dot{\zeta}^* = 0$, observe that the condition $\dot{\zeta}_1^* = 0$ implies that $\zeta_2^* = 0$. The component of acceleration due to thrust is unaffected by this condition, whereas the component due to drag becomes $d(\zeta_2^* = 0) = a$. The constant drag component corresponds to the blue dashed lines in Figure 2. The red dashed lines correspond to the velocity and acceleration of the system when drag is zero.

Enforcing the equilibrium conditions $\zeta_2^* = \dot{\zeta}_2^* = 0$ yields $d(0) - \tau(\zeta_1^*, \phi) = a - \tau(\zeta_1^*, \phi) = A\cos(2\pi\zeta_1^*/L - \phi) - 1 = 0$.

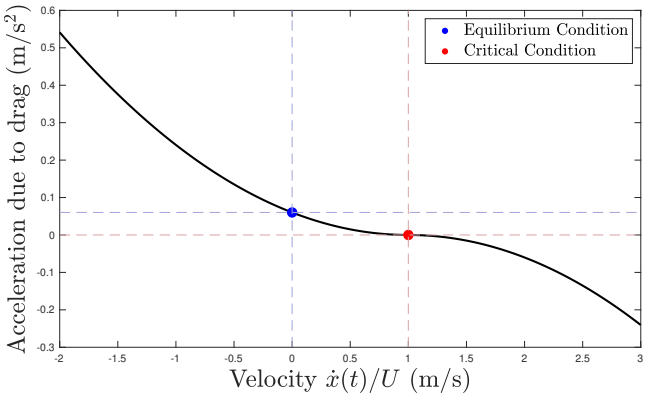

Fig. 2: Acceleration due to drag $d(\dot{x})$. Blue markers indicate the effect of drag when the system is in equilibrium. Red marker indicates the critical value where the drag is zero. Plotted using the value a = 0.0601 m/s^2.

Solving for ζ_1^* gives $\zeta_1^* = \frac{L}{2\pi}[\cos^{-1}(1/A) + \phi]$. We assign the inverse cosine term the notation $\theta = \cos^{-1}(1/A)$.

Note that, in order for an equilibrium to exist, we require $|1/A| < 1$. In terms of physical parameters, this implies $A_2 < 2A_1$, i.e., the tailbeat amplitude of the downstream fish cannot exceed twice the tailbeat amplitude of the upstream fish. Additionally, the θ value is not unique; there are two solutions for θ in every L-period of ζ_1 in the first and fourth quadrants. Because $2\pi\zeta_1/L$ appears within a cosine term in the equations of motion, ζ_1 can be thought of as an element of the unit sphere S^1, with periodic behavior, rather than an element of the real line, $\mathbb{R}^1$. As a consequence, the location and behavior of equilibrium points are also periodic.

B. Open-Loop Stability Analysis

The local stability of the equilibrium points can be determined by linearizing the system about each point and evaluating the eigenvalues of the Jacobian matrix. The relevant partials required for this process evaluate to

$$\left.\frac{\partial \tau(\zeta_1)}{\partial \zeta_1}\right|_{\zeta^*} = \frac{8\pi a}{AL}\sin(\theta) = \pm\frac{8\pi a}{A^2 L}\sqrt{A^2-1} \quad (6)$$

$$\left.\frac{\partial d(\zeta_2)}{\partial \zeta_2}\right|_{\zeta^*} = -\frac{2a}{U} \quad (7)$$

In (6), the positive value corresponds to $\theta = \cos^{-1}(1/A) \in (0, \frac{\pi}{2})$ and the negative value corresponds to $\theta \in (-\frac{\pi}{2}, 0)$. Throughout this paper, $\pm$ notation will imply this relationship between θ and the sign of the value, whereas $\mp$ notation will imply the inverse relationship. The Jacobian of the system $\dot{\zeta} = f(\zeta)$ is $\left.\frac{\partial f}{\partial \zeta}\right|_{\zeta^*}$, which evaluates to

$$\left.\begin{pmatrix} 0 & 1 \\ -\frac{\partial t(\zeta_1)}{\partial \zeta_1} & \frac{\partial d(\zeta_2)}{\partial \zeta_2} \end{pmatrix}\right|_{\zeta^*} = \begin{pmatrix} 0 & 1 \\ \mp\frac{8\pi a}{A^2 L}\sqrt{A^2-1} & -\frac{2a}{U} \end{pmatrix}.$$

By inspection, the trace of the matrix (8) is negative and the sign of the determinant is positive when $\left.\frac{\partial \tau(\zeta_1)}{\partial \zeta_1}\right|_{\zeta^*} > 0$ and negative when $\left.\frac{\partial \tau(\zeta_1)}{\partial \zeta_1}\right|_{\zeta^*} < 0$. We, therefore, expect to see a series of alternating stable equilibrium points and unstable saddle points, L-periodically. The stable equilibrium points correspond to the evaluation of $\theta = \cos^{-1}(1/A)$ in the first quadrant, whereas the unstable equilibria correspond to the evaluation in the fourth quadrant.

The resulting pattern of equilibrium points are shown in Figure 3. Changing the parameter ϕ shifts equilibrium points along x; changing the parameter A changes the spacing between alternating points.

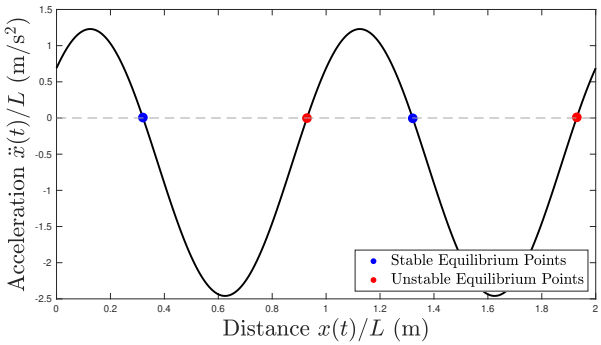

Fig. 3: Evaluating the acceleration function $\ddot{x}$ when $\dot{x} = 0$ shows the location and stability of equilibrium points in the open-loop dynamics. Plotted using the values a = 0.0601 m/s^2, $A = 3$, and $\phi = \pi/4$.

C. Open-Loop Phase Portrait

We illustrate the open-loop analysis by creating a phase portrait using the following system parameters: $A = 3$, $\phi = \pi/4$ rad, $U = 0.08$ m/s, $a = 0.0601$ m/s^2, and $L = 0.0435$ m. The phase portrait is shown over two periods in Figure 4. As expected, we see a pattern of alternating stable equilibrium points and unstable saddle points along the $\dot{x} = 0$ line, which align with those seen in Figure 3. For this particular set of parameters, we see that the stable points are spirals, which can be verified by checking that the determinant of (8) is greater than one-fourth of the trace squared.

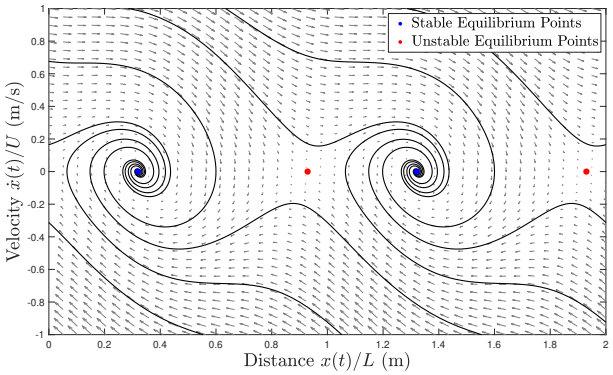

Fig. 4: Phase portrait of the open-loop dynamics.

The equilibrium distances depend on the flapping phase offset ϕ. The goal of the next section is to stabilize the swimmers to a desired inline distance apart by adjusting the phase shift, ϕ, using feedback control.

IV. Linear Feedback Control

This section derives a feedback control law to stabilize the swimmers to a desired inline separation distance. We first define where the control input $u(t)$ enters the system and modify the dynamics accordingly. Then we derive a linear control law and prove that the closed-loop system is stable.

A. Closed-Loop State-Space System

In Section III, the phase offset between the upstream and downstream swimmer was considered a system parameter. However, $\dot{\phi}(t)$ is a natural choice for a control input as it is a variable that the swimmer can manipulate directly and variations in the derivative of the phase, as opposed to the phase itself, prevent sudden changes in swimming behavior. To accommodate the addition of an input term, a new state ζ_3 is added to the two-dimensional state-space system from (5) to become the three-dimensional state-space system

$$\dot{\zeta}_1 = \zeta_2, \quad \dot{\zeta}_2 = d(\zeta_2) - \tau(\zeta_1, \zeta_3), \quad \dot{\zeta}_3 = u(\zeta), \tag{8}$$

where $\zeta_3 = \phi$. To simplify the closed-loop analysis, we shift the system such that the origin is an equilibrium point. Observe that $\dot{\zeta}_1^* = 0$ implies $\zeta_2^* = 0$ and $\dot{\zeta}_3^* = 0$ implies $u(\zeta^*) = 0$. The equilibrium condition $\dot{\zeta}_2^* = 0$ implies $2\pi\zeta_1^*/L - \zeta_3^* = \cos^{-1}(1/A) = \theta$. Depending on whether θ is a realization of $\cos^{-1}(1/A)$ in the first or fourth quadrant, the equilibrium condition describes a manifold of stable or unstable equilibrium points, respectively. Thus, for any reference inline separation distance x_{ref}, the corresponding phase offset such that the system is in equilibrium is $\zeta_3^* = \phi_{\text{ref}} = 2\pi x_{\text{ref}}/L - \theta$.

Now define the state vector $y(t) = \zeta(t) - \zeta^*$, where ζ^* is an equilibrium point with $\zeta_1^* = x_{\text{ref}}$ as

$$y_1 = \zeta_1 - x_{\text{ref}}, \quad y_2 = \zeta_2, \quad y_3 = \zeta_3 - \phi_{\text{ref}}. \tag{9}$$

Taking the derivative of each term in (9) and plugging in (8) yields the following state equations for $y(t)$:

$$\dot{y}_1 = y_2, \quad \dot{y}_2 = d(y_2) - \tau(y_1, y_3 - \theta), \quad \dot{y}_3 = u(y). \tag{10}$$

Redefining the system this way allows us to create a control law to stabilize the origin without explicit reference to the desired separation distance x_{ref}.

B. Proportional Feedback Law

As already noted, the natural dynamics of the open-loop system have stable equilibrium configurations that depend on the phase offset between the swimmers. A simple solution to realize a desired configuration x_{ref} is to apply a proportional control law to shift the phase offset.

Theorem 1. *The proportional feedback control law*

$$u(y) = -\mu y_3, \qquad \mu > 0 \tag{11}$$

asymptotically stabilizes the origin of the system (10).

Proof. To apply Lyapunov's indirect method, consider the eigenvalues of the Jacobian of $\dot{y} = g(y)$, i.e.,

$$\frac{\partial g}{\partial y} = \begin{pmatrix} 0 & 1 & 0 \\ -\frac{\partial \tau(y_1, y_3-\theta)}{\partial y_1} & \frac{\partial d(y_2)}{\partial y_2} & -\frac{\partial \tau(y_1, y_3-\theta)}{\partial y_3} \\ 0 & 0 & -\mu \end{pmatrix}.$$

Evaluating the partials found in (6) and (7) along with $\left.\frac{\partial \tau(y_1, y_3-\theta)}{\partial y_3}\right|_{y^*=0} = \mp\frac{4a}{A^2}\sqrt{A^2-1}$, the Jacobian of the closed-loop dynamics using the control law (11) evaluated at the origin is

$$\left.\frac{\partial g}{\partial y}\right|_{y^*=0} = \begin{pmatrix} 0 & 1 & 0 \\ -\frac{8\pi a}{A^2 L}\sqrt{A^2-1} & -\frac{2a}{U} & \frac{4a}{A^2}\sqrt{A^2-1} \\ 0 & 0 & -\mu \end{pmatrix}.$$

The eigenvalues of this matrix are (details omitted):

$$\begin{aligned} \lambda_{1,2} &= \frac{-aA^2L \pm \sqrt{aA^2L(aA^2L - 8\pi U^2\sqrt{A^2-1})}}{A^2LU} \\ \lambda_3 &= -\mu. \end{aligned}$$

All the system parameters that appear in these terms are positive real numbers, therefore each eigenvalue is guaranteed to have a negative real component. □

Intuitively, the state feedback input (11) smoothly shifts the equilibrium inline distances and then relies on the natural dynamics to stabilize that configuration. Indeed, the eigenvalues $\lambda_{1,2}$ of the closed-loop system are the same as those of the open-loop system. This means that, for sufficiently large gain μ, the convergence rate of the closed-loop system under proportional feedback control is fixed by the open-loop system. One option to address this is adding y_1 and y_2 terms to the control law, i.e., $u = -\mu_1 y_1 - \mu_2 y_2 - \mu_3 y_3$. Alternatively, we examine a nonlinear control design that locally preserves the dynamics and illustrates the underlying structure of the system.

V. Nonlinear Feedback Control

This section identifies an idealized Hamiltonian system and uses it to find a nonlinear feedback control law that stabilizes the origin of the system (10). We prove that the closed-loop system is locally stable and show simulated results.

A. Idealized Hamiltonian System

To improve the convergence rate of the open loop dynamics, we seek a Lyapunov-based control. Unlike a linear feedback control, this design would have the benefit of accounting for nonlinear system behavior far from the equilibrium points. It is challenging, however, to derive a useful Lyapunov function for the full closed-loop dynamics. Instead, consider a simplified version of the system.

As discussed in Section III, at the equilibrium condition where $\zeta_2^* = y_2^* = 0$, the drag effect contributes a constant term $d(0) = a$ to the acceleration. Suppose the drag is constant. Under this condition, the state-space system in y coordinates becomes

$$\begin{aligned} \dot{y}_1 &= y_2 \\ \dot{y}_2 &= \frac{4a}{A^2}\left[A\cos\left(\frac{2\pi y_1}{L} - y_3 + \theta\right) - 1\right] \\ \dot{y}_3 &= u(y) \end{aligned}$$

Consider the substitutions $z_1 = 2\pi y_1/L - y_3$ and $z_2 = y_2$. The new state-space system is now only two dimensional:

$$\dot{z}_1 = \frac{2\pi z_2}{L} - u(z), \quad \dot{z}_2 = \frac{4a}{A^2}\left[A\cos(z_1 + \theta) - 1\right] \tag{12}$$

Notice that, in the unforced system, the origin $z^* = 0$ is an equilibrium point. Furthermore, (12) is Hamiltonian, with

$$H(z_1, z_2) = \frac{\pi z_2^2}{L} + \frac{4a}{A^2}\left[z_1 - A\sin(z_1 + \theta)\right] \tag{13}$$

satisfying $\dot{z}_1 = \frac{\partial H}{\partial z_2}$ and $\dot{z}_2 = -\frac{\partial H}{\partial z_1}$. This Hamiltonian structure comes from the assumption that the drag term is constant. There cannot be any nodes or spirals in (12), only centers or saddle points [12]. This model is non-physical and neglects some of the system dynamics. However, the modified system captures the system behavior local to some of the equilibrium points and the resulting Hamiltonian conveniently acts as a Lyapunov function that we use to design a nonlinear control law.

B. Lyapunov-Based Control Law

This subsection uses Lyapunov-based analysis and LaSalle's invariance principle to design a nonlinear control law that stabilizes the origin of system (12).

Theorem 2. *The feedback control law*

$$u(z) = -\gamma\left[A\cos(z_1 + \theta) - 1\right] \tag{14}$$

for $\gamma > 0$ asymptotically stabilizes the origin of (12).

Proof. Consider the candidate Lyapunov function $V(z) = H(z) - H(0)$, i.e.,

$$V(z) = \frac{\pi z_2^2}{L} + \frac{4a}{A^2}\left[z_1 - A\sin(z_1 + \theta) + \sqrt{A^2 - 1}\right]. \tag{15}$$

By construction, (15) satisfies $V(0) = 0$. Let domain D satisfy $V(z) > 0$ for $z \in D\backslash\{0\}$. To show D exists, consider the case $z_2 = 0$, which produces the smallest evaluations of $V(z)$. If $V(z_1, 0) = \frac{4a}{A^2}\left[z_1 - A\sin(z_1 + \theta) + \sqrt{A^2 - 1}\right] > 0$ within a neighborhood of z_1, then this condition is satisfied. Notice that at $z = 0$, $V = 0$, $\frac{\partial V}{\partial z_1} = 0$, and $\frac{\partial^2 V}{\partial z_1^2} = \frac{4a\sqrt{A^2-1}}{A}$. As long as $A > 1$, $\frac{\partial^2 V}{\partial z_1^2} > 0$ making $z_1 = 0$ a local minima of $V(z_1, z_2 = 0)$, which means the domain exists.

Next apply the control law (14) to take the time derivative of the Lyapunov candidate function along solutions of (12):

$$\begin{aligned}\dot{V}(z) &= \frac{2\pi z_2}{L}\dot{z}_2 + \frac{4a}{A^2}\left[\dot{z}_1 - A\dot{z}_1\cos(z_1 + \theta)\right] \\ &= -\gamma\left[A\cos(z_1 + \theta) - 1\right]^2\end{aligned}$$

The time derivative is negative semi-definite, so the origin is stable [13]. To show that the origin is in fact asymptotically stable, we apply LaSalle's invariance principle [13]. Consider the compact set $\Omega_\epsilon = \left\{z \,\middle|\, \|z\| \le \epsilon\right\}$, where ϵ is chosen such that $V(z) \ge 0\ \forall\ z \in \Omega_\epsilon$ and $\cos(z_1 + \theta) = 1$ only once in the domain. In this domain, let $E = \left\{z \in \Omega_\epsilon \,\middle|\, \dot{V}(z) = 0\right\}$, which is equivalent to $E = \left\{z \in \Omega_\epsilon \,\middle|\, z_1 = 0\right\}$, the portion of the z_2 axis that falls in Ω_ϵ.

In order for a solution to remain in E for all time, we need $z_1 = \dot{z}_1 = 0$. This condition implies that

$$\dot{z}_1 = \frac{2\pi a z_2}{L} + \gamma\left[A\cos(0 + \theta) - 1\right] = \frac{2\pi a z_2}{L} = 0.$$

The only solution in this set is the origin. □

Recall that control law (14) is designed for the idealized dynamics (12). Because the structure of the Hamiltonian system is similar to the full non-idealized dynamics, particularly near equilibrium points, we conjecture it is an effective control law for the original system as well. Additionally, notice that the origin $z = 0$ corresponds to $2\pi\zeta_1/L - \zeta_3 = \theta$ and $\zeta_2 = 0$ in the original ζ coordinates. Because of our choice of variables, the desired value x_{ref} does not influence the origin in the z coordinates. Consequently, the control law in (14) can stabilize the system to the stable manifold, but not to a specific configuration on the manifold. For this reason, it is useful to test a control law that incorporates both (11) and (14) recast into y coordinates to account for nonlinear dynamics, while still maintaining the ability to stabilize to a specific reference value on the stable manifold.

C. Hybrid Control Law

We now examine the behavior of the closed-loop system (10) when a controller is designed incorporating terms from both the linear (11) and nonlinear (14) control laws.

Theorem 3. *The composite control law*

$$u(y) = -\gamma\left[A\cos\left(\frac{2\pi y_1}{L} - y_3 + \theta\right) - 1\right] - \mu y_3 \tag{16}$$

for $\mu, \gamma > 0$, asymptotically stabilizes the origin of (10).

Proof. Local stability of the origin is established using Lyapunov's indirect method. We already derived all the partials of $\dot{y}_1$ and $\dot{y}_2$. Now including the partials $\frac{\partial u(y)}{\partial y_1}$ and $\frac{\partial u(y)}{\partial y_3}$ to the Jacobian yields (see proof of Theorem 1)

$$\left.\frac{\partial g}{\partial y}\right|_{y^*=0} = \begin{pmatrix} 0 & 1 & 0 \\ -\frac{8\pi a}{A^2 L}\sqrt{A^2-1} & -\frac{2a}{U} & \frac{4a}{A^2}\sqrt{A^2-1} \\ \frac{2\pi\gamma}{L}\sqrt{A^2-1} & 0 & -\gamma\sqrt{A^2-1} - \mu \end{pmatrix}. \tag{17}$$

The characteristic polynomial of the Jacobian (17) is

$$\lambda^3 + b_2\lambda^2 + b_1\lambda + b_0 = 0, \tag{18}$$

where coefficients b_0, b_1, and b_2 are

$$\begin{aligned} b_0 &= \frac{8\pi a\mu\sqrt{A^2-1}}{A^2 L}, \\ b_1 &= \frac{8\pi a\sqrt{A^2-1}}{A^2 L} + \frac{2a}{U}\left(\gamma\sqrt{A^2-1} + \mu\right), \\ b_2 &= \frac{2a}{U} + \gamma\sqrt{A^2-1} + \mu. \end{aligned}$$

The Routh-Hurwitz condition [14] states that, if $b_0, b_1, b_2 > 0$ and $b_1 b_2 > b_0$, then the system is Hurwitz [14]. Each of the terms in the coefficients represent physical parameters with positive values, so the first condition is satisfied. To see that the second condition is satisfied, note that

$$\begin{aligned} b_1 b_2 &= \left[\frac{2a}{U} + \gamma\sqrt{A^2-1}\right] b_1 + \mu b_1 \\ &= \left[\frac{2a}{U} + \gamma\sqrt{A^2-1}\right] b_1 + \frac{2a\mu}{U}\left(\gamma\sqrt{A^2-1} + \mu\right) + b_0. \end{aligned}$$

The first two terms are positive, making $b_1 b_2 > b_0$. Thus, the linearized system is Hurwitz. □

D. Simulation Results

Next, we simulate the system (10) using the control law (16). The desired inline separation distance is set to $x_{\text{ref}} = 0.4L \approx 0.0174$m with gain parameters $\mu = 0.4$ and $\gamma = 0.2$. The remaining system parameters match Section III.

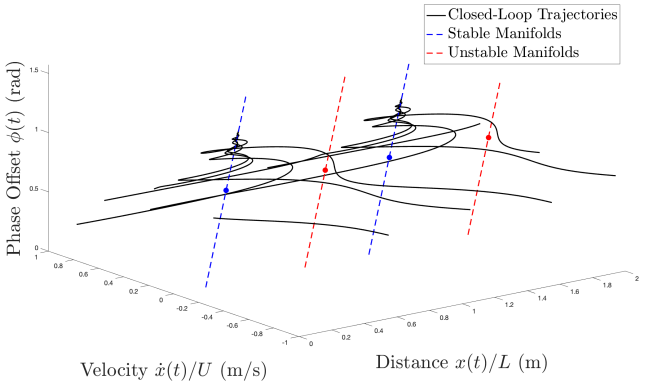

Fig. 5: Three-dimensional phase portrait of closed-loop trajectories: blue and red dashed lines show the continuum of stable and unstable equilibrium points (respectively); black curves show sample trajectories in phase-space.

Figure 5 shows a three-dimensional phase portrait of the closed-loop system. This plot is an extension of the two-dimensional phase portrait in Figure 4, which shows equilibrium points and sample trajectories when the phase is held constant at $\phi = \pi/4$. Figure 5 extends into a third dimension to reflect how the phase and, consequently the equilibrium condition, changes with feedback control. As a visual reference, the blue and red dots correspond to the points shown in Figure 4. The blue and red dashed lines show the continuous set of stable and unstable equilibrium points that arise as the phase offset is shifted. Trajectories, shown in solid black lines, converge to one of the blue lines such that $x_\infty = x_{\text{ref}} + LN, N = 0, \pm1, \pm2, \dots$ as a consequence of the L-periodic behavior inherent to the system.

To gain a deeper insight into the behavior of the trajectories presented in Figure 5 and to show the time scale, Figure 6 displays each of the three states in a single sample trajectory plotted against time along with their corresponding desired steady-state values, indicated by dashed lines.

VI. Conclusion

This paper presents a control-theoretic analysis of an experimentally validated model of inline swimming. We derive and verify linear, nonlinear, and combined control laws to achieve a desired swimming configuration between two fish swimming inline. Ongoing work includes finding a Lyapunov function that proves stability of the closed-loop system and applying this control law to an intermittently flapping downstream swimmer. Intermittent flapping allows sensors on a downstream robotic fish to obtain more accurate measurements. Determining success of control to stabilize the inline swimming configuration under these conditions is a practical concern for implementation on robotic platforms.

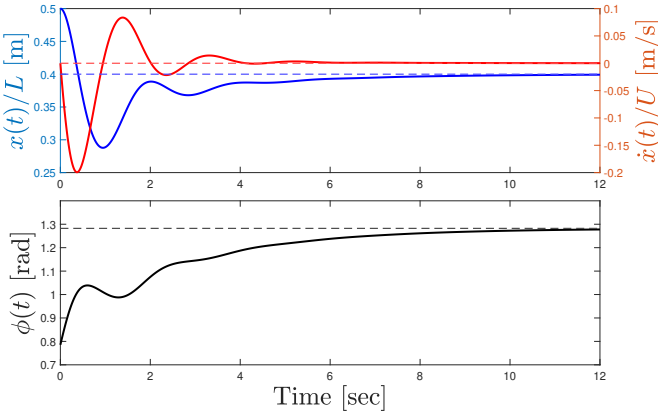

Fig. 6: Each state of a sample trajectory plotted against time: dashed lines correspond the desired configuration.

References

[1] J. C. Liao and O. Akanyeti, "Fish swimming in a Kármán vortex street: Kinematics, sensory biology and energetics," *Marine Technology Society Journal*, vol. 51, p. 48–55, Sept. 2017.

[2] J. C. Liao, D. N. Beal, G. V. Lauder, and M. S. Triantafyllou, "Fish exploiting vortices decrease muscle activity," *Science*, vol. 302, p. 1566–1569, Nov. 2003.

[3] U. K. Müller, "Fish 'n flag," *Science*, vol. 302, p. 1511–1512, Nov. 2003.

[4] M. Sfakiotakis, D. M. Lane, and J. B. C. Davies, "Review of fish swimming modes for aquatic locomotion," *IEEE Journal of Oceanic Engineering*, vol. 24, no. 2, pp. 237–252, 1999.

[5] N. E. Leonard, D. A. Paley, F. Lekien, R. Sepulchre, D. M. Fratantoni, and R. E. Davis, "Collective motion, sensor networks, and ocean sampling," *Proceedings of the IEEE*, vol. 95, p. 48–74, Jan. 2007.

[6] J. W. Newbolt, J. Zhang, and L. Ristroph, "Flow interactions between uncoordinated flapping swimmers give rise to group cohesion," *Proceedings of the National Academy of Sciences*, vol. 116, p. 2419–2424, Jan. 2019.

[7] A. D. Becker, H. Masoud, J. W. Newbolt, M. Shelley, and L. Ristroph, "Hydrodynamic schooling of flapping swimmers," *Nature Communications*, vol. 6, Oct. 2015.

[8] S. Heydari, H. Hang, and E. Kanso, "Mapping spatial patterns to energetic benefits in groups of flow-coupled swimmers," *Submitted*, Aug. 2024.

[9] X. Zhu, G. He, and X. Zhang, "Flow-mediated interactions between two self-propelled flapping filaments in tandem configuration," *Physical Review Letters*, vol. 113, Dec. 2014.

[10] L. Li, M. Nagy, J. M. Graving, J. Bak-Coleman, G. Xie, and I. D. Couzin, "Vortex phase matching as a strategy for schooling in robots and in fish," *Nature Communications*, vol. 11, Oct. 2020.

[11] H. Hang, S. Heydari, and E. Kanso, "Flow sensing and feedback control for maintaining school cohesion in uncoordinated flapping swimmers," in *2024 American Control Conference (ACC)*, pp. 3960–3965, 2024.

[12] S. H. Strogatz, *Nonlinear dynamics and chaos*. Philadelphia, PA: Westview Press, Dec. 2000.

[13] H. K. Khalil, *Nonlinear Systems*. Upper Saddle River, NJ: Pearson, 3 ed., Dec. 2001.

[14] M. Bodson, "Explaining the Routh–Hurwitz criterion: A tutorial presentation [focus on education]," *IEEE Control Systems Magazine*, vol. 40, no. 1, pp. 45–51, 2020.